Observed aerosol-layer depth at Station Nord in the high Arctic

Gryning, Sven-Erik; Batchvarova, Ekaterina; Floors, Rogier; Münkel, Christoph; Sørensen, Lise Lotte; Skov, Henrik

Published in:
International Journal of Climatology

Link to article, DOI:
10.1002/joc.8027

Publication date:
2023

Document Version
Publisher's PDF, also known as Version of record

Received: 9 March 2022 | Revised: 7 January 2023 | Accepted: 29 January 2023 | Published on: 17 February 2023

DOI: 10.1002/joc.8027

RESEARCH ARTICLE

International Journal of Climatology RMetS

Observed aerosol-layer depth at Station Nord in the high Arctic

Sven-Erik Gryning[1] | **Ekaterina Batchvarova**[1,2] | **Rogier Floors**[1] | **Christoph Münkel**[3] | **Lise Lotte Sørensen**[4] | **Henrik Skov**[4]

[1]DTU Wind and Energy Systems, Technical University of Denmark, Roskilde, Denmark

[2]Climate, Atmosphere and Water Research Institute at Bulgarian Academy of Sciences (CAWRI-BAS), Sofia, Bulgaria

[3]Vaisala GmbH, Hamburg, Germany

[4]iClimate, Arctic Research Center, Department of Environmental Science, Aarhus University, Aarhus, Denmark

Correspondence
Sven-Erik Gryning, DTU Wind and Energy Systems, Technical University of Denmark, Roskilde, Denmark.
Email: sveg@dtu.dk

Funding information
Danish Environmental Agency Monitoring of short-lived climate components in Arctic; European Cooperation in Science and Technology, Grant/Award Number: COST Action CA18235 PROBE; National Science Fund of Bulgaria, Grant/Award Number: KP-06-N34/1; Nationalt Udvalg for Forskningsinfrastruktur (NUFI)

Abstract

The depth of the aerosol layer at the Villum Research Station at Station Nord in the high Arctic is analysed based on 8 years of observations from a ceilometer and one full year from a wind lidar. The layer is of particular interest for aerosol process modelling and atmospheric chemistry studies. The depth of the aerosol layer is assigned to the inflection point in the attenuated backscatter profile by two methods; one is based on polynomial approximation of the profile and the other is direct numerical differentiation. The analysis is based on two types of hourly profiles; one consists of averaging the attenuated backscatter observations and the other by computing the median. Due to sporadic occurrence of outliers in the ranges around 50 m in the ceilometer observations, this part of the profile is not used in this study. Restricting the observations to heights above 100 m, the depths of the aerosol layer are found to be typically ≈230 m. It varies little between winter and summer, but the spread in the depth is larger during the winter as compared to summer. To extend the study of the aerosol-layer depth below 100 m, a method is applied that combines the ceilometer measurements with the carrier-to-noise ratio from the wind lidar. The results are available for 2018 only, and they show aerosol-layer depths below ≈80 m as well as depths around 230 m and they show few observations between ≈80 and ≈230 m. Near the ground, the observed backscatter exhibits a pronounced seasonal variation, having low values during the summer and high values during the winter. The strength of the seasonal variability decreases with height, especially above the aerosol-layer depth, and is virtually absent at 1 km.

KEYWORDS

aerosol-layer depth, attenuated backscatter profiles, carrier-to-noise ratio, ceilometer, high Arctic, wind lidar

1 | INTRODUCTION

The greatest climate changes are taking place in the Arctic (Masson-Delmotte et al., 2021). Near-surface climate warming has proceeded at approximately three times the global average rate since 1980. This extraordinary rate of warming, named the Arctic amplification, has been recognized since the late 1990s (Serreze et al., 2000) and has accelerated since Bekryaev et al. (2010) and Box et al. (2019). Large efforts are devoted to experimental work (Boy et al., 2019) to improve our understanding of the complex processes that control Arctic amplification and meteorology. Chemistry and aerosols play a significant role in the Arctic amplification, but a generally acknowledged understanding has not yet been reached of the sources of the vertical distributions. In this study we investigate the statistic of the surface-based aerosol layer. The layer defines the volume available for surface-sourced gases or aerosols, and thus is of particular interest for atmospheric chemistry, and aerosol process studies and modelling. It is a characteristic feature for the Arctic that the air near the surface is predominantly stably stratified during a large part of the year, and vertical profiles of temperature are predominantly characterized by the presence of temperature inversions (Vihma et al., 2003). In general, such very stable boundary layers are poorly characterized and poorly understood (Mahrt et al., 2009). The Arctic inversion effectively shields the Arctic surface from the free atmosphere. It is shallow, believed to be typically a few hundreds of meters or less, and dynamically isolated from the free atmosphere. During the Arctic summer melt, the surface temperature can be locked to the melting point of ice, and sensible turbulent fluxes of heat in the atmosphere do not respond directly to changes in the incoming radiative forcing (Persson, 2012). Instead, horizontal advection and clouds have a greater control over the boundary-layer structure (Nilsson, 1996; Overland, 1985; Persson et al., 2002; Tjernström, 2005; Tjernström et al., 2015). During the Arctic winter darkness and early spring, low levels of short-wave solar radiation and the high surface albedo of snow minimize the heating of the surface, creating extended periods of high thermostatic stability and strong surface inversions. During weak winds the suppression of turbulence by buoyancy is larger than the production by wind shear; as a result, the turbulence vanishes. Under such conditions, additional processes appear to govern the boundary-layer structure. Elevated layers of turbulence may be generated by breaking gravity waves (Sun et al., 2015), by wind shear in low-level jets and drainage flows (Garratt, 1994).

In the traditional sense, following Seibert et al. (2000), the boundary layer is the layer that is influenced by the surface, and its depth is thus the upper lid to which pollutants or aerosols, emitted near ground level, are dispersed. The most direct way to measure the depth of the boundary layer will be from profile of meteorological measurements, which can be achieved in campaigns using aircraft (Suomi et al., 2016) and by measurements at tall meteorological towers. Standard radio soundings also provide direct measurements of the meteorological parameters, but the observations are often not suited for studies of the lowest part of the atmosphere due to the coarse vertical resolution. Instead, high-resolution specialized boundary-layer soundings are carried out (Batchvarova et al., 2014), but usually in short-term intensive measurement campaigns only. However, all methods are cumbersome especially in the Arctic because of the hostile environments and remote locations with challenging access conditions.

Alternative methods originate in the aerosol layer that is often found close to the ground, where the aerosol concentration is generally considerably higher than in the free atmosphere. Relating the boundary-layer height with the depth of the aerosol layer has fostered the development of a multitude of methods to determine the boundary-layer depth focusing on the mid-latitude with a clear daily variation in the surface fluxes. These methods are fundamentally based on tank experiments by Deardorff et al. (1980) on the structure of the convective boundary layer. Deardorff et al. (1980) found the top of the mixed-layer "to agree roughly with the height at which mixed-layer fluid occupies one-half the area." In the threshold method, which was proposed by Melfi et al. (1985), the top of the aerosol layer (boundary layer) is assigned to the height of the layer close to the ground, where the attenuated backscatter reaches a fixed threshold. In the gradient method put forward by Endlich and Ludwig (1979), the lowest inflection point in the attenuated backscatter profile is taken as an indication of the top of the mixed layer. It can be found by direct numerical differentiation of the attenuated backscatter profile. Other methods along this line are suggested by Davis et al. (2000) and Brooks (2003) by estimating the depth of the mixed layer applying a discrete Haar or multiple dilations wavelet transforms to the inflection point.

The use of remote sensing instruments, in particular ceilometers, in the Arctic has mainly dealt with cloud base height measurements. Ceilometers have some advantages as compared to dedicated aerosol lidars, such as relatively continuous operations and low-maintenance, eye-safety and comparatively low price, which compensates for the disadvantages of lower maximum range and relatively low signal-to-noise ratio. These advantages have resulted in an increasing use of ceilometers in studies related to boundary-layer height research

(e.g., Avolio et al., 2017; Caicedo et al., 2017; Di Giuseppe et al., 2012; Eresmaa et al., 2006; Ketterer et al., 2014; Lotteraner & Piringer, 2016; Münkel, 2007; Uzan et al., 2016; Zhu et al., 2016).

Reflecting the relative novelty of the ceilometer for Arctic research applications, there exists a number of publicly available data sets that have not yet been fully exploited, such as on ceilometer backscatter, cloud base height and cloud fraction data during the Arctic Ocean 2018 expedition (Prytherch & Tjernström, 2020). Ceilometer cloud base height measurements taken at Summit Station, Greenland, as part of the Arctic Observing Network program were made available by Shupe (2010) in the Arctic Data Center depository, and ceilometer data from the cruise of the German ship Polarstern in 2020 into the Arctic Ocean are found in the PANGAEA depository (Schmithüsen, 2021).

In this manuscript, we investigate the seasonality of the attenuated backscatter and the depth of the aerosol layer in the high Arctic based on an 8-year data set of observations from a ceilometer supplemented by 1 year of measurements from a wind lidar at Station Nord (Villum Research Station). It is emphasized that the aerosol layer is not necessarily turbulent. The depth of the aerosol layer is estimated from a (1) polynomial approximation and by a (2) direct numerical differentiation of the averaged, as well as the median of the attenuated backscatter profiles and at lower heights we also use 1 year of results from a wind lidar.

FIGURE 1 Map of the area north of the Arctic Circle (66°30′N) showing the position of the Villum Research Station at Station Nord. The Arctic Circle limits the area with polar night and midnight sun often considered as the Arctic region

2 | SITE

Villum Research Station is located at Station Nord, on Princess Ingeborg Peninsula (Danish: Prinsesse Ingeborg Halvø) in northern Crown Prince Christian Land (Danish: Kronprins Christian Land), in Northeastern Greenland at position 81°36′N 16°40′W. Except for the Canadian station Alert on Ellesmere Island, it is the world's northernmost permanent settlement, located just 930 km from the North Pole and 1700 km north of the Arctic Circle (Figure 1). The nearest towns are Longyearbyen on Svalbard, 720 km east of the station, Ittiqqortoormiit in Greenland is 1250 km to the south and Thule Air base is 1200 km southwest of Station Nord. It is not accessible by ship, as ice conditions would only permit a passage once every 5–10 years. A meteorological observatory, radar station and an air strip were built at Station Nord by the United States in the 1950s as an emergency runway for polar flights during the Cold War. The United States soon realized that they no longer needed the airfield. It was handed over to the Danish state in 1952, which kept its location secret until the National Geographic Magazine showed the location on one of its maps. It was closed in 1972 but reopened in 1975 as a support base for the dog sledge Sirius patrol that enforce national sovereignty in these remote and uninhabited parts of Greenland.

Since 1990, air pollution measurements have been carried out and since 1996 an air pollution monitoring station named Flyger's Hut has operated 2.5 km north of the central complex of buildings. Station Nord was also frequently used as a gateway to the otherwise inaccessible portions of northeastern Greenland for national and international scientific expeditions. In 2015, a substantial upgrade of the complex was achieved by the construction of a new research infrastructure, Villum Research Station (VRS), including a new monitoring house. It is the property of the Greenland Government, represented by the Greenlandic Institute of Natural Resources and is being managed by Aarhus University in Denmark. The station is open for access throughout the year. The station hosts individual scientific projects focusing on atmospheric, marine and terrestrial research. In addition to this, the station is also used as a permanent base for an extensive long-term monitoring station within the Arctic Monitoring and Assessment Programme (AMAP; www.amap.no). The Aerosol, Cloud, Trace gases Research InfraStructure (ACTRIS; www.actris.eu) and the Integrated Carbon

Observation System (ICOS; www.icos-cp.eu) all report scientific data, besides the mentioned programs to the European Monitoring and Evaluation Program (EMEP) and WMO-Global Atmosphere Watch (WMO-GAW).

VRS features a very cold polar tundra climate (ET in the Köppen–Geiger classification; Köppen, 1936) with average temperatures just a few degrees above freezing during the short summer and very cold winters. The temperature is generally low with a climatologically mean of −16.9°C. The month with the highest daily mean temperature of 3.4°C is July and the coldest is March with −30.7°C. It is a very dry climate with annual precipitation of 188 mm having a minimum of 11 mm in January and maximum of 23 mm in April. A full climatology can be found in Cappelen et al. (2001). The area around VRS is rather flat with a glacier tongue stretching into the sea towards the west. Knuths fjeld, a hill in the range of 100 m, is situated a few kilometres to the south. Towards east the isolated ice cap Flade Isblink reaches a height of approximately 700 m. The inland ice is more than 100 km south of the station. More details on the landscape are available in Goodsite et al. (2014) and Gryning et al. (2021).

3 | MEASUREMENTS

The analysis presented in this paper is based on remote sensing of the atmosphere carried out by two distinctly different instruments. One is the Vaisala CL51 laser diode ceilometer. While originally designed for detection of cloud base layers (e.g., Gryning et al., 2021), it is widely used for automatic monitoring of the height of the atmospheric boundary layer (Kotthaus et al., 2020). The other remote sensing instrument is a Wind Cube V2 Doppler wind lidar, which has obtained widespread use in the wind industry. Although their potential in basic boundary-layer research has been the focus for intensive efforts in several COST (Cooperation in Science and Technology) Actions (e.g., Cimini et al., 2020; Illingworth et al., 2015), they are still considered underexploited.

Operation of the CL51 ceilometer at Station Nord began in 2011. Since 20 August 2017 a V2 Doppler Wind lidar has been operating in parallel with the ceilometer at VRS. The analysis reported in this study covers data from 12 May 2011 until 12 April 2019.

3.1 | Ceilometer

A CL51 ceilometer consists of a vertically pointing laser and a receiver in the same location. A laser pulse with a wavelength of 905 nm and a duration of 100 ns is transmitted every 100 μm. As the beam travels through the atmosphere, tiny fractions of the light are scattered by aerosols. Generally, the size of the particles in question are similar in size to the wavelength of the laser (Mie scattering). A small component of the scattered light is directed back to the lidar receiver. The backscattered signal is received by an Avalanche Photo Diode detector and recorded. The timing is transformed into height and in this way, each laser pulse results in a vertical profile of the backscattered signal. Pulses are emitted with a frequency of 10 kHz for about 1.6 s followed by a period of 0.4 s to run the firmware algorithm and store the data. The CL51 ceilometers have a single lens optical design using the outer part for receiving and the inner part of the lens for transmitting light. In this way, overlap of the transmitter light cone and the receiver field-of-view is obtained over the whole measuring range and sufficient overlap for aerosol layer investigations is reached at low ranges from the first or second range gate upward (Münkel et al., 2011). Details of near-range ceilometer attenuated backscatter profiles are given in Wiegner et al. (2014) and Kotthaus et al. (2016).

Operation of the CL51 ceilometer at VRS involves averaging in time and range. The report interval for the backscatter profiles was set to 60 s; profile range resolution is 10 m and a maximum range of 13,000 m with the first observation level at 10 m. From 20 March to 22 August 2013 the instrument was undergoing maintenance in Denmark and as part of this service the temporal resolution was increased to 16 s and the maximum measuring height was changed to 7700 m. The vertical resolution remained unchanged at 10 m.

Inspection of the measurements revealed that the ceilometer has problems at distinct ranges close to the ground. Unphysical deviations at 50 m in both the mean and median backscatter profile are clearly visible in Figure 2a,b. The 50 m glitch is often seen at CL51. Its amplitude is instrument-specific and varies with temperature, so there is no simple way to correct for it in the ceilometer firmware. The reason for the 50 m switch is some tiny receiver voltage disturbance caused by triggering the laser pulse. The backscatter signal from 50 m is collected just a few nanoseconds after that trigger. Furthermore, in the lowest two range gates, there are irregular signal fluctuations that are caused by the heater being switched on and off at more or less regular time intervals. Wiegner et al. (2014) also questioned the range gates up to 60 m.

3.2 | Doppler wind lidar

Doppler wind lidars are a relatively new technique for obtaining wind measurements by benefitting from the

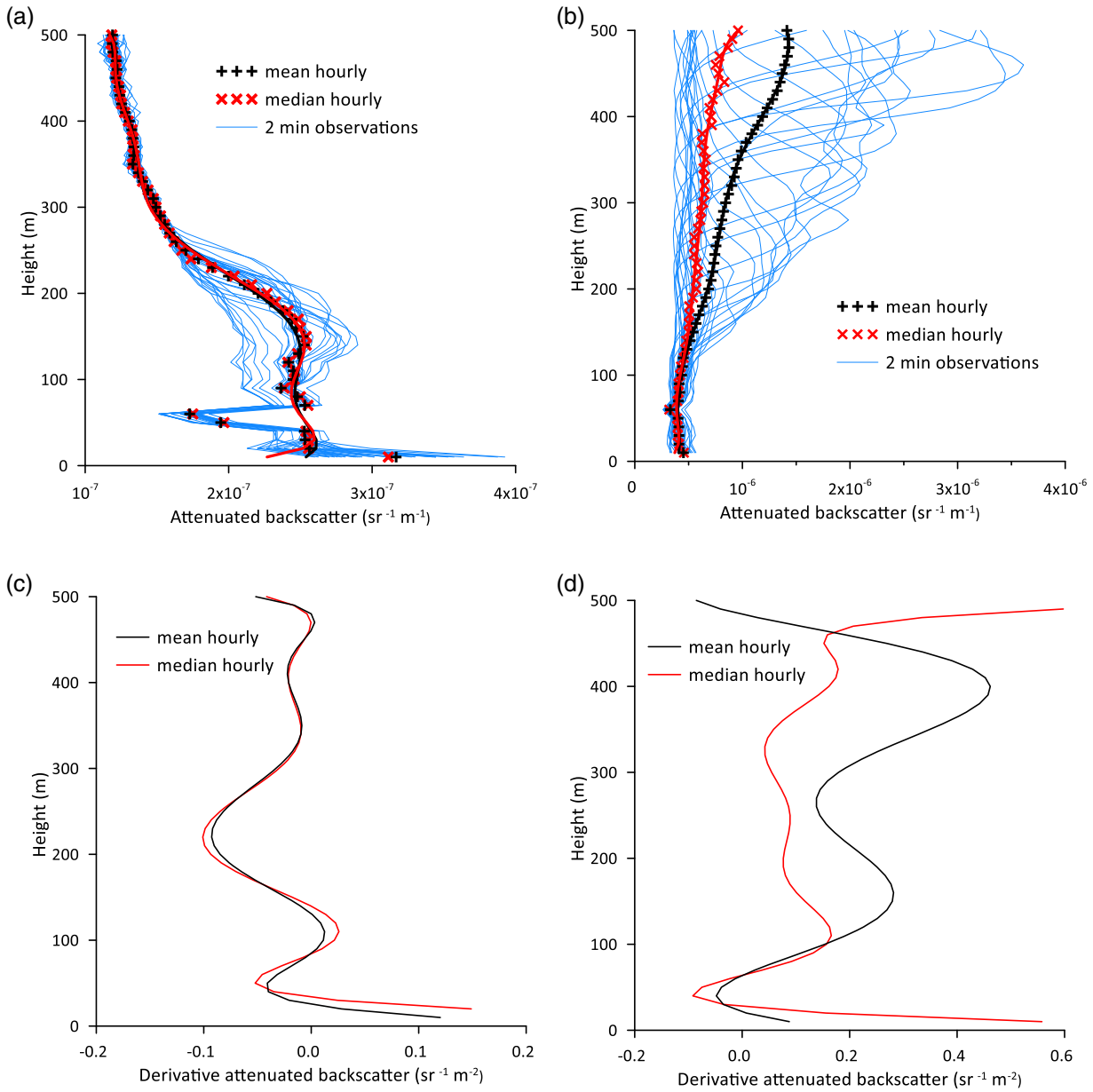

FIGURE 2 Examples of profiles of attenuated backscatter measured by the ceilometer. In Figure 2a, the attenuated backscatter profile is near constant in a layer close to the ground and then decreases as it approaches the backscatter in the free atmosphere. It is possible for this type of profiles to assign a depth to the aerosol layer. This is illustrated in Figure 2c showing the first order derivative with height of the attenuated backscatter profile. The aerosol-layer depth is assigned to ≈220 m as indicated by the minimum in the first order derivative. Figure 2b shows a profile that is increasing with height thus having a predominantly positive first-order derivative as illustrated in Figure 2d. For such profile types, there is no depth of the aerosol layer. Outliers in both profiles around the 50 m range gate of the ceilometer can be observed. The panels represent observations between 1–2 o'clock on 31 August 2018 (left panels) and 1–2 o'clock on 7 January 2018 (right panels). The black crosses represent hourly averages, and the red ones represent the median of the observations. The full lines represent the polynomial approximations to the mean (black) and median (red) and the blue lines are 2-min observations

development of optical fibre amplifiers. It is an active remote instrument that transmits pulses of light that are backscattered by particles in the air. Wind lidars rely on the backscattered Doppler shifted laser light and in this way they measure radial velocities as function of height. To retrieve the horizontal flow field, a sequence of radial velocities measured by beams from different directions are required. Several scanning modes have been developed, for example, Doppler Beam Swinging (DBS; Pauscher et al., 2016), Velocity Azimuth Display (VAD; Lhermite, 1962) and Range Height Indicator (Sathe & Mann, 2013), making a Doppler wind lidar a very

versatile instrument for wind profile research. Contrary to many meteorological instruments, the Doppler wind lidar provides a quality indicator for the observations, the so-called carrier-to-noise ratio (CNR). High values of the CNR indicate observations with a high accuracy and decreasing values of the CNR gradually suggest a higher uncertainty (Gryning & Floors, 2019).

In this study, a V2 Doppler wind lidar manufactured by Leosphere is used. It transmits pulsed beams of light with a wavelength of 1540 nm in four perpendicular directions (DBS scanning) with an angle from the vertical of 28°, as well as in the vertical direction with a data output frequency of 1 Hz. The reporting of data consists of 1 Hz data of radial winds and CNR as well as 10 min averages of the horizontal wind speed and direction, the vertical wind speed and the carrier-to-noise ratio from 40 to 200 m in ranges of 20 m.

4 | DERIVATION OF THE DEPTH OF THE AEROSOL LAYER

Analysis presented here on the depth of the aerosol layer is based on hourly averaged profiles of attenuated backscatter from the ceilometer derived from the raw measurements. In order to exclude cases of low clouds, precipitation and fog from the analysis, only profiles where all values in the hourly averaged attenuated backscatter between 100 and 500 m are less than $2{\cdot}10^{-5}$ $sr^{-1}{\cdot}m^{-1}$ are considered (e.g., Gryning et al., 2021). Fulfilling this condition discards 15% of the profiles.

4.1 | Data treatment

Averaging is preferable, as the raw data can contain spurious data that at least in part will be diminished during the averaging process. On the other side a long averaging time will mask the finer structure of the profiles that can be physical in nature. Traditionally, the profiles represent the mean of the attenuated backscatter derived over the averaging time (e.g., Kotthaus et al., 2020). In this way, averaging includes all measurements. An alternative way is to derive the profile as the median of the measurements over the averaging time. This method also embraces all the measurements but will very effectively remove large and small outliers, as well as large physical derivations that might exist from the mean profile. Here both types of hourly profiles are applied.

It was found that for most cases, the profile of the attenuated backscatter, up to several hundreds of meters, is well represented by the generic profile shown in Figure 2a. The hourly averaged aerosol concentration is relatively high close to the ground, remaining near constant up to some height where the aerosol concentration starts to decrease and finally reaches the low value in the free air above the boundary layer. It can be noticed that despite the mean and median profiles are different they have the same overall vertical structure. In this case, the 2-min averaged profiles show a considerable scatter inside the aerosol layer and have little variability outside. The scatter inside the aerosol layer is not random but constitute a gradual change in the profile over time. Not all profiles can be represented by this general description; some were found to deviate considerable by, for example, increasing from the ground and upward and never showing a decreasing trend within the considered vertical range, or by a more complex and less structured profile. Figure 2b shows an example of the former for the mean and median profiles of the attenuated backscatter. It can be observed that overall, the same shape is found for both profiles despite noticeable differences in the actual backscatter between the mean and median profiles. The 2-min averaged profiles have very similar shapes with distinct peaks with low backscatter below and above. The peaks are descending over time, which can be expected from a discrete source of aerosols or entraining air from the free atmosphere.

Inspection of the measurements show unphysical deviations at 50 m in both the mean and median backscatter profile as clearly visible in Figure 2a,b. In an attempt to remove this effect a filter was applied to the profile such that no measurements were allowed to deviate more than 10% from their adjoined neighbours. When this is the case, the mean of its lower and higher neighbours replaced the measurement. Still, even after this filtering, the measurements near the ground were noisy or irregular; therefore, the analysis is restricted to measurements from 100 m and above.

Here, a method is devised to study the part below 100 m in the profile of the attenuated backscatter from the ceilometer by including observations from a wind lidar that is operated at VRS since August 2017. Output from the wind lidar contains the so-called CNR (carrier-to-noise ratio) as a function of height, which is related to the strength of the backscatter of the wind lidar signal and used to assign a quality indicator to the observed wind speed. The outgoing laser beam is focused to improve the carrier-to-noise ratio at ranges close to the focal length and thus used to improve the Doppler wind lidar velocity data quality and data availability. The optimal choice of focus will depend on the atmospheric conditions at the deployment location (Hirsikko et al., 2014). Calculating attenuated backscatter from the carrier-to-noise ratio requires knowledge of the telescopic focus function for the specific wind lidar, which is usually not available. As the CNR observations (units of dB) represent the logarithm of

backscatter, the relative attenuated backscatter coefficient $\beta(z)$ for the wind lidar can be expressed as

$$\beta(z) \propto 10^{(\mathrm{CNR}(z)-f(z))}, \quad (1)$$

where $\mathrm{CNR}(z)$ is the carrier-to-noise ratio at height z and $f(z)$ is the telescope function of the wind lidar, both in dB. Here we estimated the telescope function based on homogeneous profiles of aerosols (attenuated backscatter) from the ceilometer. A large number of profiles of ceilometer observations with near constant observations of the attenuated backscatter between 10 m and well above 200 m are selected and compared to the corresponding $\mathrm{CNR}(z)$ profiles. Each of the selected ceilometer profiles with constant attenuated backscatter is compared to the corresponding CNR profile, and the difference between the CNR at 100 m and CNR at height z is calculated. Next, the average value of all the estimates of the $\mathrm{CNR}(100)-\mathrm{CNR}(z)$ is calculated for each height z, which constitute the correction to the observed CNR that is required in order to achieve a constant profile of the focus corrected CNR for such cases where the profile of the attenuated backscatter from the ceilometer is constant. The estimated discrete values of the relationship between height and $\mathrm{CNR}(z)$ (Figure 3) shows that the focal length of the wind lidar is about 100 m, and that $\mathrm{CNR}(z)$ correction decreases when moving up or down from the focal length. It should be noted that the attenuated backscatter when derived from Equation (1) from attenuated backscatter ceilometer profiles in this way is not only focus corrected but also range corrected.

The focus and range corrected carrier-to-noise ratio, $\mathrm{CNR}(z)-f(z)$, is used to derive the pseudo attenuated backscatter profile by use of Equation (1). Figure 4 shows the observed attenuated backscatter from the ceilometer plotted as function of corrected carrier-to-noise ratio for observations from 60, 100 and 200 m heights. An empirical relationship between the attenuated backscatter and the corrected CNR profile is proposed

$$\ln(\beta(z)) = 0.0062x^2 + 0.3958x - 9.4503, \quad (2)$$

where the corrected CNR is denoted x, thus $x = \mathrm{CNR}(z) - f(z)$. Next, a time-series of pseudo attenuated backscatter profiles from hourly $\mathrm{CNR}(z)$ observations were derived by use of Equation (2).

4.2 | Aerosol-layer depth

Here we apply a method to estimate the height of the boundary layer that is frequently used with low power lidars such as ceilometers. It is based on the determination of the inflection points of the backscatter profile. The aerosol backscatter signal depends on the aerosol numerical concentration and in a rather complicated way also on aerosol size, shape and composition. Humidity may cause a change in backscatter with altitude for hygroscopic aerosols, which will swell in size as relative humidity increases. If the size, shape and composition can be considered uniform in space, the volume aerosol backscatter coefficient, determined from the lidar measurements, can be considered linearly proportional to the aerosol number.

Having derived the filtered data set, the next step is to approximate a higher-order polynomial to each of the filtered backscatter profiles. A polynomial approximation acts as an additional filter on the backscatter profile. A lower-order polynomial will blur physically fine structures of the profile, while a high-order not only will be representative for the physical profile, but will add also some of the inevitable noise. The method that is used to estimate the depth of the aerosol layer is based on best-fit polynomials (in a least-squares sense) for hourly averaged and median attenuated backscatter profiles. It turned out that for these observations an 8th or 9th degree polynomial approximation provided a good fit to the data. The degree of the polynomial approximation was estimated by finding a fit that provided the smallest spread across the depth in the histogram of the aerosol

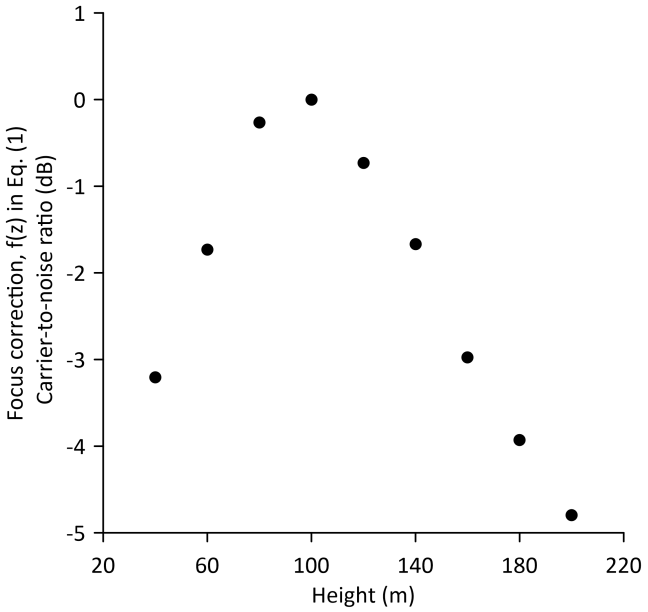

FIGURE 3 Illustration of the height dependence of the carrier-to-noise ratio observations from the wind lidar for ceilometer profiles with near constant attenuated backscatter between 10 and 200 m. The relationship, shown as discrete values for the height ranges of the wind lidar, corresponds to $f(z)$ in Equation (1)

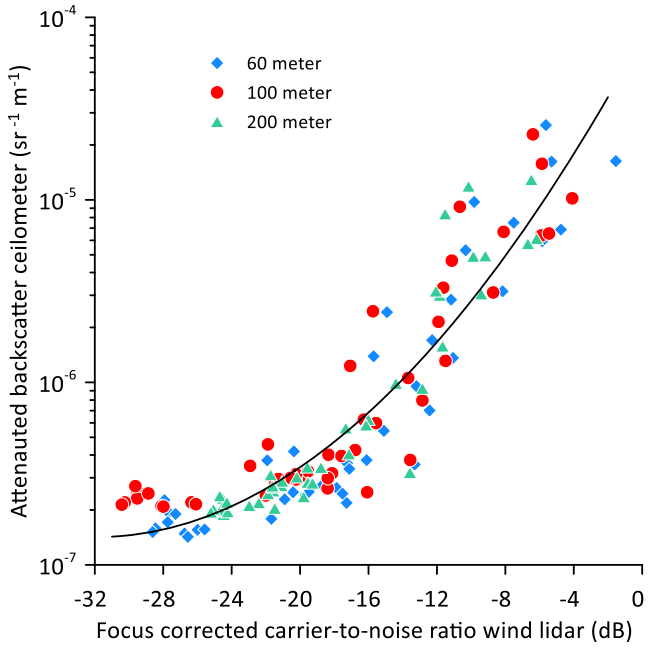

FIGURE 4 Relationship between the focus corrected carried-to-noise ratio from the wind lidar (CNR$(z)-f(z)$, and the attenuated backscatter observations by the ceilometer. The observations represent bi monthly averages from August 2017 to April 2019

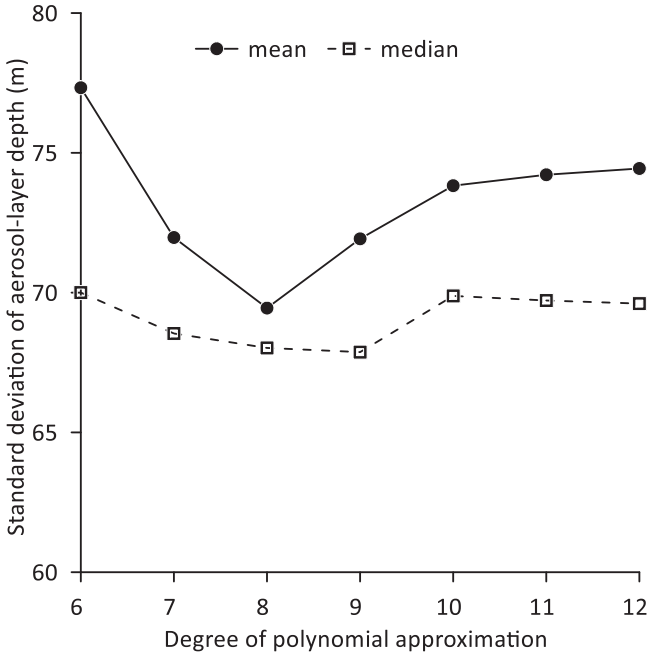

FIGURE 5 Standard deviation of the depth of the aerosol layer as a function of the degree of the polynomial approximation. Filled circles are based on the mean profiles and squares on the median profiles of the attenuated backscatter

layer. It should be noted that a perfect fit to the observations could not be achieved because it would introduce additional noise from the observations in the fitted profile. Figure 5 illustrates that the standard deviation of the depth of the aerosol layer reaches a minimum for a polynomial of degree 8 when applied to mean profiles and a degree of 9 for median profiles. It can be noted that using a degree of 8 or 9 for both types of profiles (mean and median) leads to very minor differences.

The height of the aerosol layer was assigned to the height of the smallest negative (largest negative value in absolute terms) first-order derivative of the polynomial with respect to height that was also an inflection point—i.e., having a second-order derivative near zero. It was not unusual that several inflections were found and in these cases the height of the aerosol layer was assigned to the height with the smallest negative first derivative. Alternatively, the depth of the aerosol layers was estimated by a traditional method based on direct numerical differentiation of the profile of the attenuated backscatter. However, before applying the method, the measurements were filtered with a moving average of three height ranges.

The attenuated backscatter profile needs to fulfil certain requirements with respect to its overall shape to be able to assign the depth of the aerosol layer. It was found that in several cases, the backscattered profiles were irregular or constantly increasing with height which indicated lack of an aerosol-layer depth in the attenuated backscatter profile. Figure 2a,c shows an example of a profile with an aerosol-layer depth at ≈220 m, as can be seen in the well-defined minima in the first derivative. A considerable variability in the 2-min observations below the aerosol-layer depth and little variability above can be noted. Figure 2b,d illustrates a profile, where a depth of the aerosol layer does not exist. Those 2-min observations with high aerosol concentrations are associated with a descending aerosol-loaded air mass that lasted about 15 min, indicating entrainment from the troposphere.

5 | CLIMATOLOGY OF THE AEROSOL LAYER

An example of backscatter profiles up to 1000 m over a period of 2.5 days, in April 2012, is shown in Figure 6. It can be observed that the profile exhibits a clear structure such that the attenuated backscatter is near constant up to 250 m, then it decreases and becomes near constant further above. The diamond and cross symbols illustrate the depth of the aerosol layer derived from hourly averages of the mean and median profiles by the method of polynomial approximation.

Having shown an example of a near stationary 2.5-day time series of the attenuated backscatter, the

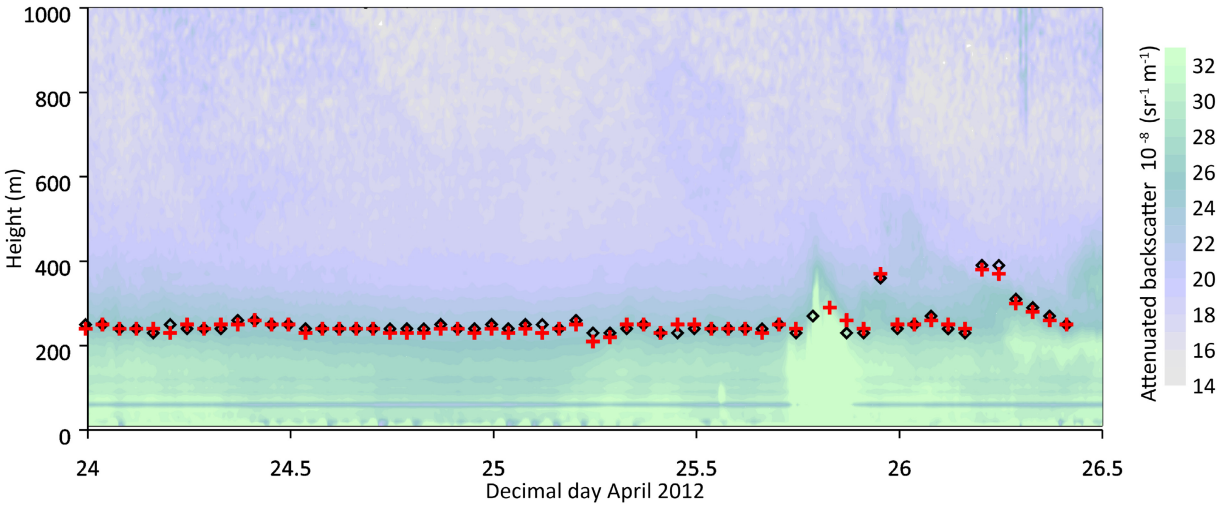

FIGURE 6 Example of the temporal evolution of the depth of the aerosol layer. Observations are from a period where the sun is visible throughout the whole period and the surface is snow-covered. The black diamonds mark the estimated depth of the aerosol layer when derived from hourly profiles of the mean of the observations of the attenuated backscatter, and the red crosses from profiles of the median of the observations. The aerosol depth is derived by using the polynomial approximation. As already pointed out in Figure 2, outliers exist and in this case at a height of about 50 m. They are seen here as a blue horizontal stripe

long-term behaviour is demonstrated by plotting the monthly median for a number of heights for the whole observing period (Figure 7). Near the surface, a pronounced annual variation can be observed with a maximum during winter and a minimum, being about 10 times smaller, during summer months. This is in agreement with earlier observations of particle size distribution number concentration (Nguyen et al., 2016; Pernov et al., 2022) and confirms that Station Nord (VRS) is located north of the summer extent of the Arctic front, which hinders long range transport of accumulation mode particles (those that provide the backscatter of the lidars) from mid-latitudes to VRS. It provides the possibility to study the aerosol-layer depth at both high (winter) and low (summer) concentrations. The annual variation decreases with altitude, particularly above the mean depth of the aerosol layer, in agreement with the general picture that the Arctic front forms a dome above the Arctic where pollutants can be transported aloft (e.g., Jiao & Flanner, 2016). To illustrate the observations further, a histogram of the depth of the aerosol layer, using the measurements during summer and winter in 2018, is shown in Figure 8. Here we apply definitions of the seasons at VRS following Gryning et al. (2021), where the seasons are defined according to the sun's position relative to the horizon. Summer is defined as the period from 10 April to 3 September, where the sun is up all day and winter as the period 17 October–24 February where it is down all day.

Two versions of the histograms are shown in Figure 8. In panels (a) and (b) the aerosol-layer depth is

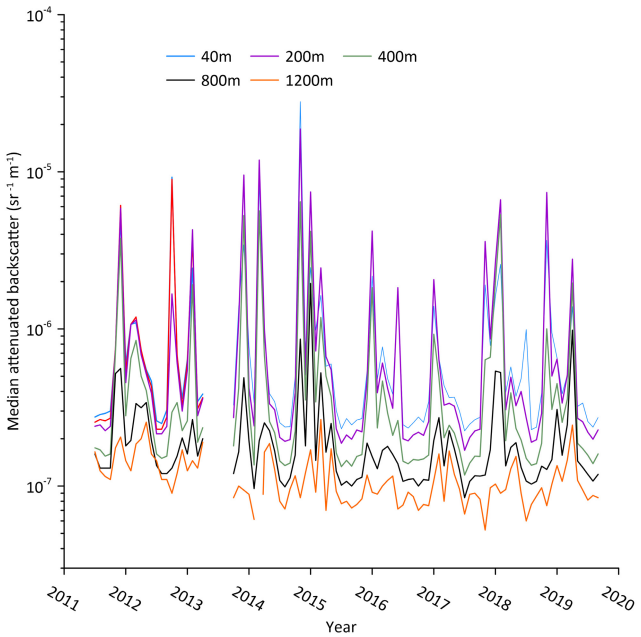

FIGURE 7 Illustration of the evolution of the monthly median of the attenuated backscatter as function of height between 40 and 1200 m. Near the surface the attenuated backscatter can be seen to be an order of magnitude higher during the winter as compared to summer conditions

derived by a polynomial approximation, and in panels (c) and (d) by numerical differentiation. It is a characteristic feature that the histogram for both summer and winter has a maximum at a depth of about 230 m as shown in (c) and (d) and 250 m as shown in (a) and (b), but the

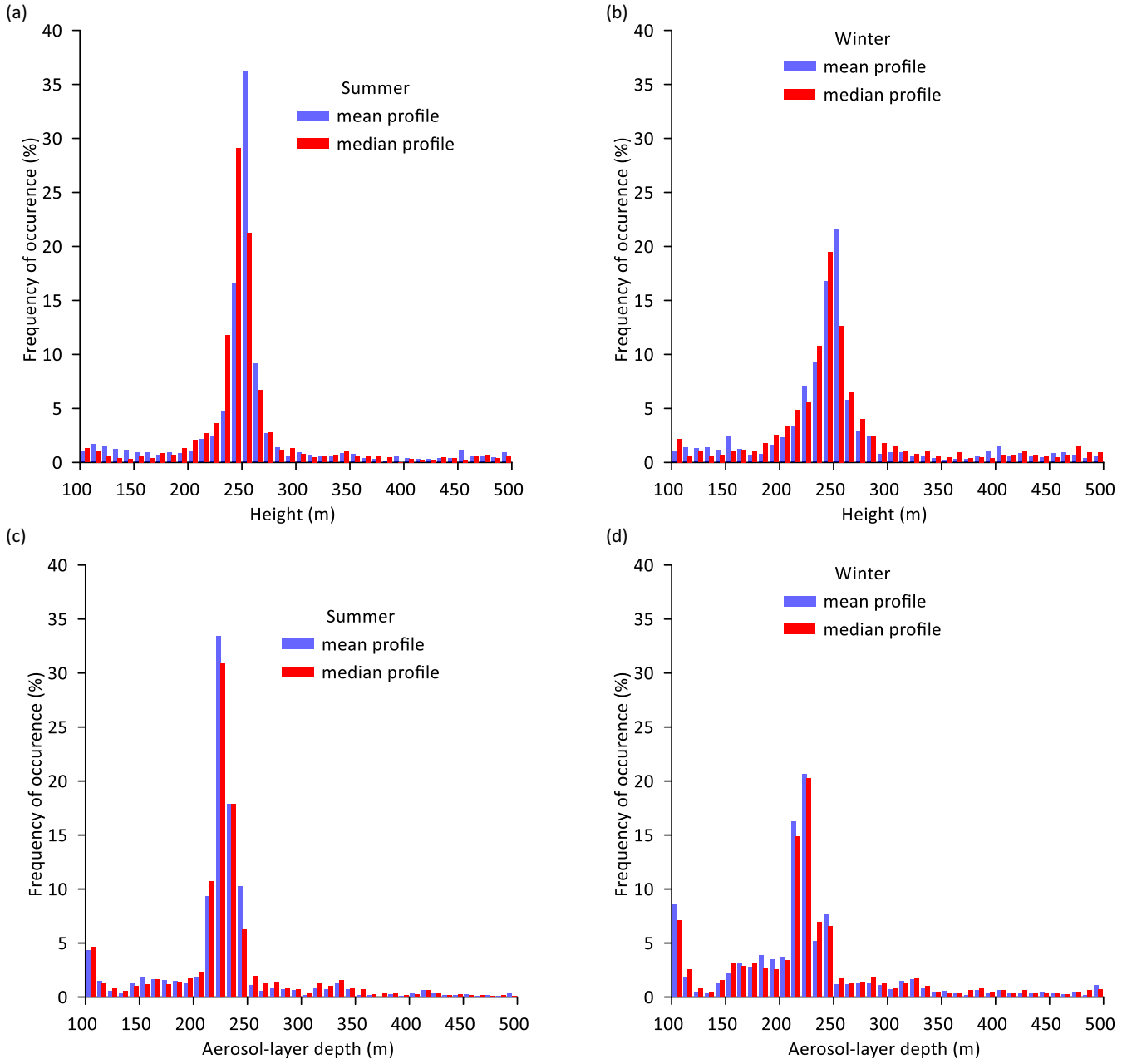

FIGURE 8 Histogram of the depth of the aerosol layer for summer (a, c) and winter (b, d) for the year 2018 based on hourly values of mean (blue columns) and median (red columns) of attenuated backscatter profiles. The upper panels (a, b) represent the best fit polynomial approximation method and the lower panels (c and d) represent the direct numerical differentiation method

width of the histogram is larger during winter than during summer in both cases. The annual variability of the depth of the aerosol layer is illustrated in Figure 9. It can be observed that the overall depth of the aerosol layer is rather similar during summer and winter with no apparent annual or seasonal trend. It is noticed that although small and comparable to the size of the ceilometer range resolution, there is a clear difference, with a consistently deeper layer in winter when using the polynomial method (Figure 9a), and a slightly less consistent deeper layer in summer when applying direct numerical differentiation (Figure 9b). Although the difference is small, it indicates that the polynomial and direct numerical differentiation approaches show opposite differences, which might be due to differences in the nature of the top of the aerosol layer during winter and summer or biases in the different methods. Figure 9c,d illustrates that the annual variation of the yearly mean is minor.

The finding in Figure 8 shows that the spread of the depth of the aerosol layer in 2018 is larger during the winter, which is found also for the other years. This is

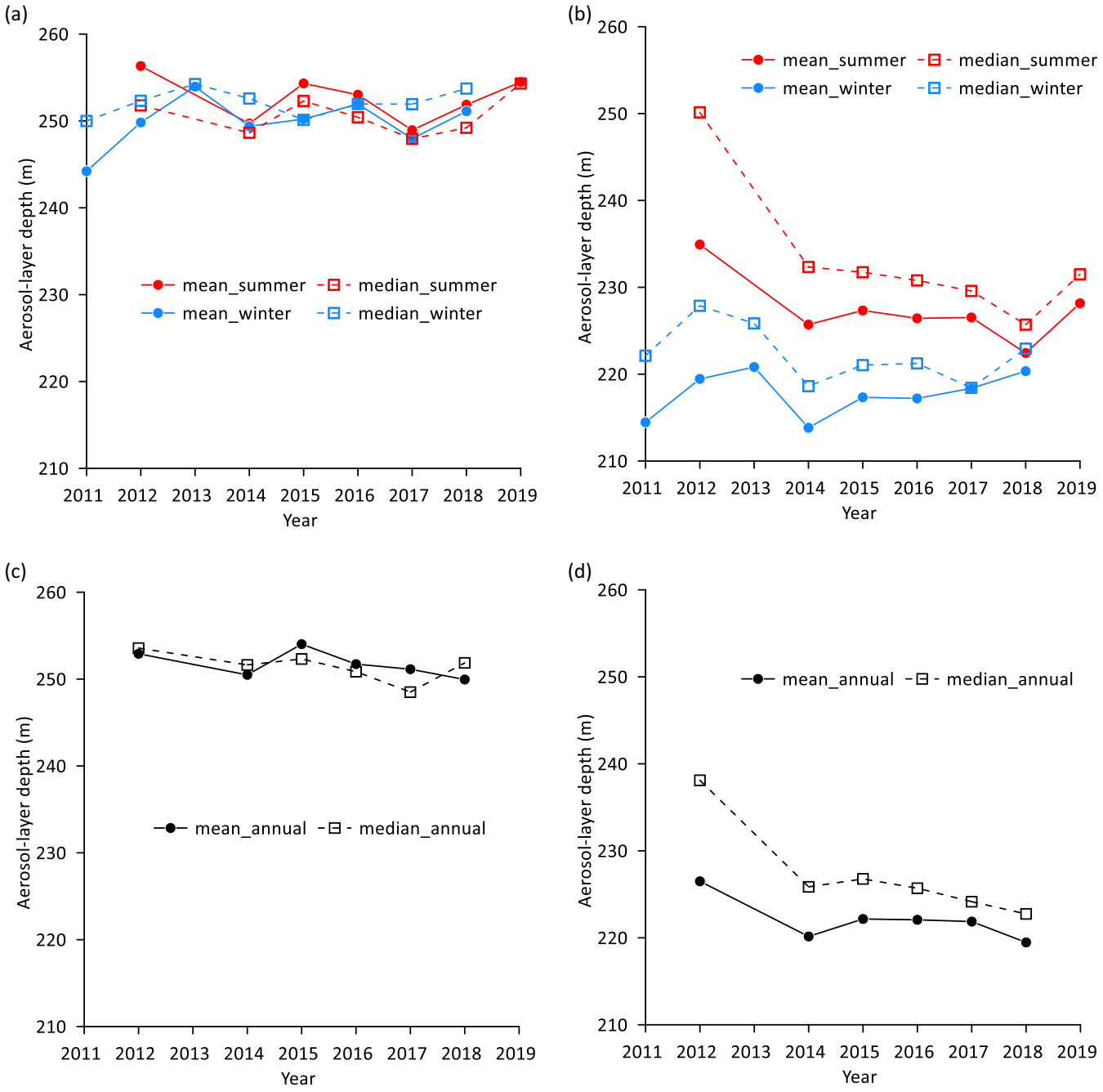

FIGURE 9 Annual variation of the mean depth of the aerosol layer for summer and winter seasons (a, b) as well as the yearly mean (c, d). Filled circles represent estimates based on mean and squares on median profiles. Red is summer, blue is winter and black is annual. In the left panels (a, c), the aerosol depth is derived by the polynomial approximation, and in the right panels (b, d), the aerosol depth is derived by the direct numerical differentiation method

illustrated by plotting the standard deviation of the distribution of the depth of the aerosol layer. Figure 10a shows it is larger during winter as compared to summer—in agreement with the findings in Figure 8.

If more than 30% of the measured ranges in the backscatter profile have a positive derivative, there is no aerosol-layer depth in the profile of the attenuated backscatter, that is, more than 30% of the backscatter profiles increase with height. The value of 30% is empirical. It was determined by scrutinizing a large number of ceilometer profiles. A threshold value of 30% was found to be adequate in order to locate profiles that did not have an aerosol-layer depth. In such profiles, the attenuated backscatter was increasing with height or with an erratic structure. Figure 11 illustrates the annual variation of such cases. The numbers are smaller during the summer compared to winter and near equal for

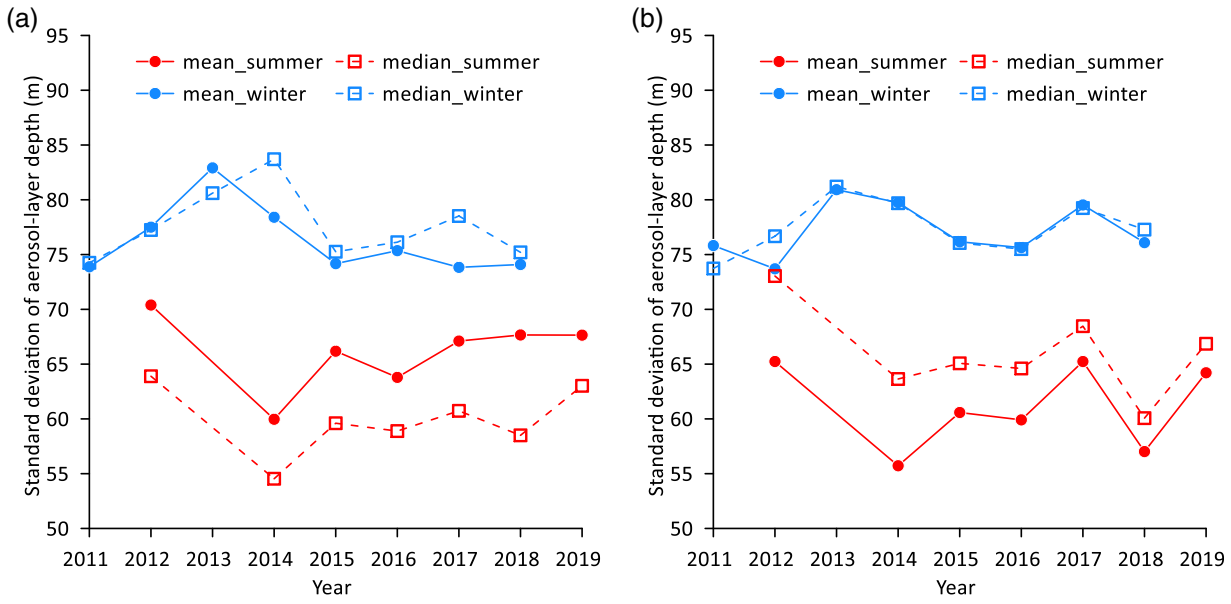

FIGURE 10 Illustration of the seasonal (summer and winter) deviation in the distribution of the depth of the aerosol layer. Panels show the standard deviation (a) for the polynomial approximation method and (b) for the direct numerical differentiation method. Symbols used are as in Figure 9

mean and median backscatter profiles. In about 20% of the profiles during summer and 30% during the winter, there is no aerosol-layer depth.

As already discussed in section 4, ceilometer observations below 100 m were excluded from the part of the attenuated backscatter profiles that constitute the basis for the results presented in Figures 8–11. In order to include the aerosol layer below 100 m in the study, data from 2018, being the only full year of parallel observations between the wind lidar and ceilometer, are applied. A method is devised that combines the ceilometer measurements with carrier-to-noise ratio observations from the wind lidar. The carrier-to-noise ratio observations, being only available between 40 and 200 m, revealed aerosol-layer depths mainly below 80 m (Figure 12). When recalling the depths ≈230 m that were found in the ceilometer profiles, this indicates the existence of a two-layer structure of the aerosol layers. A time series of the depth of the aerosol layer that is adjacent to the surface was derived by comparing simultaneous hourly averaged aerosol layers determined from the wind lidar and the ceilometer and choosing the lowest one. Figure 13 shows the histogram of the aerosol-layer depth from 2018 based on the two combined time series. It shows aerosol-layer depths below ≈80 m as well as depths around 230 m and they show few observations of aerosol-layer depths between ≈80 and ≈230 m. However, the analysis should be treated with some caution because the wind lidar and ceilometer are equipped with different types of laser sources with different wave lengths, 905 and 1540 nm, respectively.

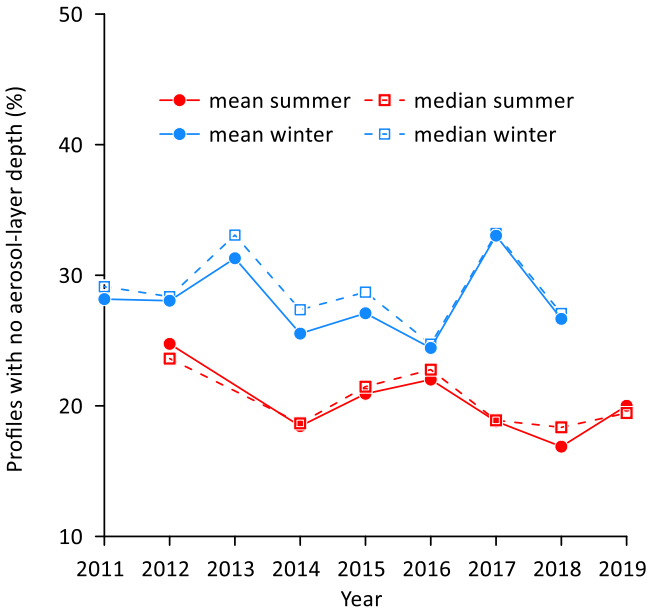

FIGURE 11 Percentage of the attenuated backscatter profiles with no aerosol-layer depth because the profiles are increasing with height or irregular. Symbols used are as in Figure 9

6 | DISCUSSION

The Arctic atmosphere is highly heterogeneous and composed of superimposed aerosol layers of different composition, origin and transport history.

There are substantial sources of aerosols in the Arctic region. Tobo et al. (2019) found glacial outwash plains to

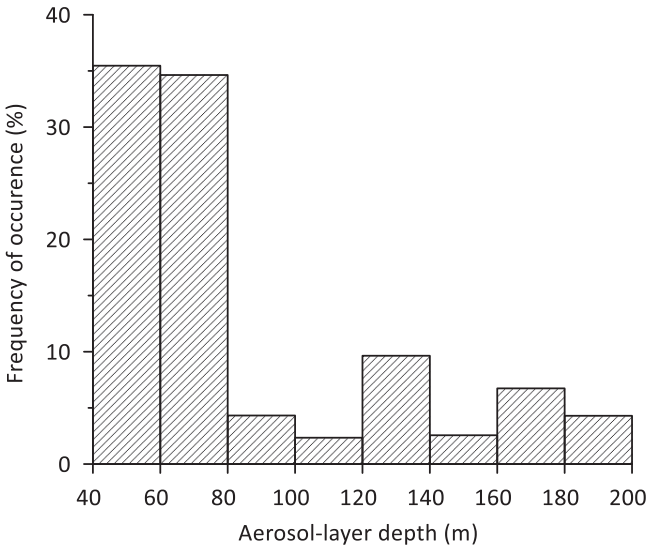

FIGURE 12 Histogram of the depth of the aerosol layer derived by numerical differentiation for year 2018 from time-series of attenuated backscatter profiles from the wind lidar

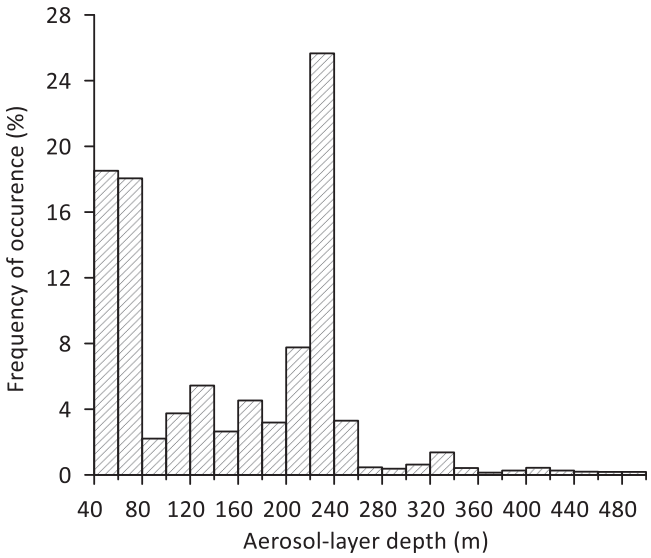

FIGURE 13 Histogram of the depth of the aerosol layer derived by numerical differentiation for year 2018 from time series of combined hourly mean values of attenuated backscatter profiles from the ceilometer and wind lidar

be a major dust source at high latitudes. Due to the recent rapid and widespread retreat of glaciers in the Arctic, dust emissions are anticipated to increase, although the effect and quantities are not well known. In Iceland dust storms are a major source of aerosols (Prospero et al., 2012). Emissions, being highest in spring, were found to be associated with active glacial outwash plains and glacial outburst floods. Pernov et al. (2022) found that in the high Arctic, fine aerosols are dominating during the winter and early spring originating from advection from long distances; later in the summer and early autumn local chemical sources for secondary aerosols take over. These are just some examples of the sources of aerosols in the Arctic. A more extensive description can be found in Tomasi et al. (2007), Dall'Osto et al. (2018), Freud et al. (2017) and Boy et al. (2019).

The composition of the lower troposphere in the Arctic is additionally controlled by long-range transport of emissions from northern Eurasia that are trapped in the Arctic thermally very stable stratified air. The strong surface inversions form shells over the Arctic, which results in the so-called Polar dome. The Polar dome is asymmetric and temporally highly variable. In addition, the Arctic lower troposphere is isolated from the lower latitudes by a transport barrier referred to as the Arctic front, which arises as a result of cold polar air meeting warm tropical air. A sharp gradient in temperature occurs at the boundary of the two air masses. Other suggestions for the boundary of the Polar dome and Arctic front are provided by Klonecki et al. (2003) and Stohl (2006).

During the winter the Arctic front can be located as far south as 40°N which allows polluted air from northern Eurasia to enter into the Arctic by low-level transport. Stohl (2006) suggested a number of pathways making it possible for the polluted air to reach the lower troposphere inside the Polar dome. During the summer the Arctic front moves northward inhibiting the transport of air masses from northern Eurasia into the Arctic (Carlson, 1981; Lutsch et al., 2020; Marelle et al., 2015; Raatz et al., 1985; Warneke et al., 2010). The northward retreat of the Arctic front is one of the reasons why aerosol concentrations in the Arctic are lower in summer than during the winter. Actually, Station Nord (VRS) is located near the northern summer extent of the Arctic front (Iversen, 1996) but still further to the north in agreement with the observed variability of the aerosol concentration (backscatter) depicted in Figure 7, and is of course well embraced by the Arctic front during winter. The implications of the generally low aerosol layers indicate that the planetary boundary layer is very shallow. This agrees with Vihma et al. (2003) that found on-ice Arctic temperature inversions to be typically ≈200 m. This should be taken into account when doing atmospheric modelling work for the VRS site and, if it is representative of a wider range of cryospheric localities (mostly surrounded by year-round ice and snow), it can have widespread importance. Specifically, care must be taken when initializing atmospheric numerical models with chemistry and aerosols both for research and weather forecasting. For back trajectory calculations for in-situ atmospheric measurements, the start height should not be more than 250 m above and preferably even at a lower level to ensure that it is representative for the measurement site.

7 | CONCLUSIONS AND IMPLICATIONS

From the analysis of ceilometer and wind lidar observations at the Villum Research Station at Station Nord in the high Arctic, it was concluded that:

- There is a considerable seasonal variability in the attenuated backscatter near the surface. The backscatter is high (high aerosol concentration) during the winter and low during the summer. This is an indication that Station Nord (VRS) is located north of the summer extent of the Arctic front.
- The seasonal variability in the attenuated backscatter gradually ceases with height especially above the aerosol-layer depth and is near absent at about 1 km in the vertical, in agreement with the general picture that the Arctic front forms a dome above the Arctic where air (clean or polluted) can be transported aloft.
- Both during winter and summer the depth of the aerosol layer could be estimated from ceilometer observations of the attenuated backscatter profiles. In this study, we applied attenuated backscatter profiles of both hourly mean and median profiles. The depth of the aerosol layer was assigned to the inflection point in the profile. It was derived by two methods (1) from polynomial approximation to the attenuated backscatter profiles and (2) by direct numerical differentiation of the profiles.
- For these observations an 8th and 9th degree polynomial approximation of the attenuated backscatter profile was found to be adequate for estimating the aerosol-layer depth from mean and median profiles respectively.
- The histogram of the depth of the aerosol layer shows a predominant maximum at about 230–250 m with little seasonal or annual variation when excluding observations below 100 m.
- The variability of the depth of the aerosol layer was larger during winter than summer.
- Although the difference is small, the aerosol layer is consistently deeper in winter when using the polynomial method and slightly deeper in summer when applying direct numerical differentiation. Thus, the polynomial and direct numerical differentiation approaches show opposite differences, which might be due to differences in the nature of the top of the aerosol layer during winter and summer or biases in the different methods.
- There is no depth to the aerosol layer for about 20% of the profiles during summer and 30% during winter. This mainly relates to backscatter profiles that are irregular in shape or increasing with height.
- A method to extend the backscatter profile below 100 m, by combining CNR observations from a wind lidar with the ceilometer observations is devised. It is applied for 2018, being the only full year with parallel observation, and found that the aerosol layer has depths below ≈80 m and at ≈230 m and few cases of depths between ≈80 and ≈230 m.
- The generally low aerosol layer at VRS should be taken into account in the initializing and in the boundary conditions when doing atmospheric modelling work that include chemistry and aerosols for the VRS site. The start height when doing back trajectory calculations for in situ atmospheric measurements should not exceed 250 m above the ground.
- It needs to be investigated if the aerosol-layer depth at VRS is representative for a wider range of cryospheric localities.

AUTHOR CONTRIBUTIONS

Sven-Erik Gryning, Ekaterina Batchvarova and Christoph Münkel provided analysis and interpretation of ceilometer attenuated backscatter profiles and drafted the manuscript. Sven-Erik Gryning performed the analysis of the wind lidar observations. Henrik Skov was lead applicant on the proposal that funded the wind lidar and Lise Lotte Sørensen on the proposal for the ceilometer, both supervised the operation of the ceilometer and wind lidar. All authors revised the article critically, approved the final version and agree to be accountable for all aspects of the work.

ACKNOWLEDGEMENTS

The Danish Environmental Agency is acknowledged for funding through the project "Monitoring of short-lived climate components in Arctic" (in Danish: Monitering af kortlivede klimakomponenter i Arktis) and the Villum Research Station for hosting the ceilometer and Doppler wind lidar. NUFI is acknowledged for support to ACTRIS DK project. Further support was achieved by the National Science Fund of Bulgaria, Contract KP-06-N34/1 "Natural and anthropogenic factors of climate change—analyzes of global and local periodical components and long-term forecasts." The work is related to activities of three of the authors (Sven-Erik Gryning, Ekaterina Batchvarova and Rogier Floors) within the COST Action CA18235 PROBE (PROfiling the atmospheric Boundary layer at European scale). This article is based upon work from COST Action CA18235 PROBE, supported by COST (European Cooperation in Science and Technology). We thank Paul Halton who kindly read through the manuscript.

ORCID

Sven-Erik Gryning https://orcid.org/0000-0001-5451-6510

REFERENCES

Avolio, E., Federico, S., Miglietta, M.M., Lo Feudo, T., Calidonna, C.R. & Sempreviva, A.M. (2017) Sensitivity analysis of WRF model PBL schemes in simulating boundary-layer variables in southern Italy: an experimental campaign. *Atmospheric Research*, 192(April), 58–71. Available from: https://doi.org/10.1016/j.atmosres.2017.04.003

Batchvarova, E., Gryning, S.-E., Skov, H., Sørensen, L.L., Kirova, H. & Münkel, C. (2014) Boundary-layer and air quality study at "Station Nord" in Greenland. In: Steyn, D.G. & Mahur, R. (Eds.) *Air pollution modeling and its applicaton XXIII*. Cham: Springer, pp. 525–529. Available from: https://doi.org/10.1007/978-3-319-04379-1_86

Bekryaev, R.V., Polyakov, I.V. & Alexeev, V.A. (2010) Role of polar amplification in long-term surface air temperature variations and modern Arctic warming. *Journal of Climate*, 23(14), 3888–3906. Available from: https://doi.org/10.1175/2010JCLI3297.1

Box, J.E., Colgan, W.T., Christensen, T.R., Schmidt, N.M., Lund, M., Parmentier, F.J.W. et al. (2019) Key indicators of Arctic climate change: 1971–2017. *Environmental Research Letters*, 14(4), 045010. Available from: https://doi.org/10.1088/1748-9326/aafc1b

Boy, M., Thomson, E.S., Navarro, J.C.A., Arnalds, O., Batchvarova, E., Bäck, J. et al. (2019) Interactions between the atmosphere, cryosphere, and ecosystems at northern high latitudes. *Atmospheric Chemistry and Physics*, 19(3), 2015–2061. Available from: https://doi.org/10.5194/acp-19-2015-2019

Brooks, I.M. (2003) Finding boundary layer top: application of a wavelet covariance transform to lidar backscatter profiles. *Journal of Atmospheric and Oceanic Technology*, 20(8), 1092–1105. Available from: https://doi.org/10.1175/1520-0426(2003)020<1092:FBLTAO>2.0.CO;2

Caicedo, V., Rappenglück, B., Lefer, B., Morris, G., Toledo, D. & Delgado, R. (2017) Comparison of aerosol lidar retrieval methods for boundary layer height detection using ceilometer aerosol backscatter data. *Atmospheric Measurement Techniques*, 10(4), 1609–1622. Available from: https://doi.org/10.5194/amt-10-1609-2017

Cappelen, J., Jørgensen, B.V., Laursen, E.V., Stanius, L.S. & Thomsen, R.S. (2001) *The observed climate of Greenland, 1958–99—with climatological standard Normals, 1961–90*. Danish Meteorological Institute. Technical report: 00-18, pp. 1–152. Available from: http://ny.dmi.dk/fileadmin/user_upload/Rapporter/TR/2000/tr00-18.pdf%0Apapers://f554698c-bc30-43aa-8c0c-c8de8adb48e4/Paper/p2894

Carlson, T.N. (1981) Speculations on the movement of polluted air to the Arctic. *Atmospheric Environment (1967)*, 15(8), 1473–1477. Available from: https://doi.org/10.1016/0004-6981(81)90354-1

Cimini, D., Haeffelin, M., Kotthaus, S., Löhnert, U., Martinet, P., O'Connor, E. et al. (2020) Towards the profiling of the atmospheric boundary layer at European scale—introducing the COST Action PROBE. *Bulletin of Atmospheric Science and Technology*, 1(1), 23–42. Available from: https://doi.org/10.1007/s42865-020-00003-8

Dall'Osto, M., Lange, R., Geels, C., Beddows, D.C., Harrison, R.M., Simo, R. et al. (2018) Regions of open water and melting sea ice drive new particle formation in the north east Greenland. *Scientific Reports*, 8, 6106.

Davis, K.J., Gamage, N., Hagelberg, C.R., Kiemle, C., Lenschow, D. H. & Sulivan, P.P. (2000) An objective method for deriving atmospheric structure from airborne lidar observations. *Journal of Atmospheric and Oceanic Technology*, 17(11), 1455–1468. Available from: https://doi.org/10.1175/1520-0426(2000)017<1455:AOMFDA>2.0.CO;2

Deardorff, J.W., Willis, G.E. & Stockton, B.H. (1980) Laboratory studies of the entrainment zone of a convectively mixed layer. *Journal of Fluid Mechanics*, 100(1), 41–64. Available from: https://doi.org/10.1017/S0022112080001000

Di Giuseppe, F., Riccio, A., Caporaso, L., Bonafé, G., Gobbi, G.P. & Angelini, F. (2012) Automatic detection of atmospheric boundary layer height using ceilometer backscatter data assisted by a boundary layer model. *Quarterly Journal of the Royal Meteorological Society*, 138(664), 649–663. Available from: https://doi.org/10.1002/qj.964

Endlich, R.M. & Ludwig, F.L. (1979) An automatic method for determining the mixing depth from lidar observations. *Atmospheric Environment*, 13, 1051–1056.

Eresmaa, N., Karppinen, A., Joffre, S.M., Räsänen, J. & Talvitie, H. (2006) Mixing height determination by ceilometer. *Atmospheric Chemistry and Physics*, 6(6), 1485–1493. Available from: https://doi.org/10.5194/acp-6-1485-2006

Freud, E., Krejci, R., Tunved, P., Leaith, R., Nguyen, Q.T., Massling, A. et al. (2017) Pan-Arctic aerosol number size distributins: seasonality and transport patterns. *ACP*, 17, 8101–8128.

Garratt, J.R. (1994) Review: the atmospheric boundary layer. *Earth Science Reviews*, 37(1–2), 89–134. Available from: https://doi.org/10.1016/0012-8252(94)90026-4

Goodsite, M., Skov, H., Asmund, G., Bennike, O., Feilberg, A., Glasius, M. et al. (2014) Pilot study of contaminants near Station Nord, a military airbase and research station in NE Greenland. In: Linkov, I. (Ed.) *Sustainable Cities and Military Installations*. NATO Science for Peace and Security Series C: Environmental Security. Dordrecht: Springer, pp. 177–198. Available from: https://doi.org/10.1007/978-94-007-7161-1_10

Gryning, S.E., Batchvarova, E., Floors, R., Münkel, C., Skov, H. & Sørensen, L.L. (2021) Observed and modelled cloud cover up to 6 km height at Station Nord in the high Arctic. *International Journal of Climatology*, 41(3), 1584–1598. Available from: https://doi.org/10.1002/joc.6894

Gryning, S.E. & Floors, R. (2019) Carrier-to-noise-threshold filtering on off-shore wind lidar measurements. *Sensors (Switzerland)*, 19(3), 592. Available from: https://doi.org/10.3390/s19030592

Hirsikko, A., O'Connor, E.J., Komppula, M., Korhonen, K., Pfüller, A., Giannakaki, E. et al. (2014) Observing wind, aerosol particles, cloud and precipitation: Finland's new ground-based remote-sensing network. *Atmospheric Measurement Techniques*, 7(5), 1351–1375. Available from: https://doi.org/10.5194/amt-7-1351-2014

Illingworth, A.J., Cimini, D., Gaffard, C., Haeffelin, M., Lehmann, V., Löhnert, U. et al. (2015) Exploiting existing ground-based remote sensing networks to improve high-resolution weather forecasts. *Bulletin of the American Meteorological Society*, 96(12), 2107–2125. Available from: https://doi.org/10.1175/BAMS-D-13-00283.1

Iversen, T. (1996) Atmospheric transport pathways for the Arctic. In: Wolff, E.W. & Bales, R.G. (Eds.) *Chemical exchange between the atmosphere and Polar snow*. NATO ASI Series (Vol. 43). Berlin, Heidelberg: Springer, pp. 71–92.

Jiao, C. & Flanner, M.G. (2016) Changing black carbon transport to the Arctic from present day to the end of 21st century. *Journal of Geophysical Research*, 121(9), 4734–4750. Available from: https://doi.org/10.1002/2015JD023964

Ketterer, C., Zieger, P., Bukowiecki, N., Collaud Coen, M., Maier, O., Ruffieux, D. et al. (2014) Investigation of the planetary boundary layer in the Swiss Alps using remote sensing and in situ measurements. *Boundary-Layer Meteorology*, 151(2), 317–334. Available from: https://doi.org/10.1007/s10546-013-9897-8

Klonecki, A., Hess, P., Emmons, L., Smith, L., Orlando, J. & Blake, D. (2003) Seasonal changes in the transport of pollutants into the Arctic troposphere-model study. *Journal of Geophysical Research*, 108, 8367. Available from: https://doi.org/10.1029/2002JD002199

Köppen, W. (1936) Das geographische System der Klimate. In: Band, I. & Teil, C. (Eds.) *Handbuch der Klimatologie*. Berlin: Verlag von Gebrüder Borntraeger.

Kotthaus, S., Haeffelin, M., Drouin, M.A., Dupont, J.C., Grimmond, S., Haefele, A. et al. (2020) Tailored algorithms for the detection of the atmospheric boundary layer height from common automatic lidars and ceilometers (Alc). *Remote Sensing*, 12(19), 1–23. Available from: https://doi.org/10.3390/rs12193259

Kotthaus, S., O'Connor, E., Münkel, C., Charlton-Perez, C., Haeffelin, M., Gabey, A.M. et al. (2016) Recommendations for processing atmospheric attenuated backscatter profiles from Vaisala CL31 ceilometers. *Atmospheric Measurement Techniques*, 9(8), 3769–3791. Available from: https://doi.org/10.5194/amt-9-3769-2016

Lhermite, R. (1962) Note on wind variability with Doppler radar. *Journal of the Atmospheric Sciences*, 19, 343–346.

Lotteraner, C. & Piringer, M. (2016) Mixing-height time series from operational ceilometer aerosol-layer heights. *Boundary-Layer Meteorology*, 161(2), 265–287. Available from: https://doi.org/10.1007/s10546-016-0169-2

Lutsch, E., Strong, K., Jones, D.B.A., Blumenstock, T., Conway, S., Fisher, J.A. et al. (2020) Detection and attribution of wildfire pollution in the Arctic and northern midlatitudes using a network of Fourier-transform infrared spectrometers and GEOS-Chem. *Atmospheric Chemistry and Physics*, 20(21), 12813–12851. Available from: https://doi.org/10.5194/acp-20-12813-2020

Mahrt, L., Thomas, C.K. & Prueger, J.H. (2009) Space-time structure of mesoscale motions in the stable boundary layer. *Quarterly Journal of the Royal Meteorological Society*, 135, 67–75.

Marelle, L., Raut, J.C., Thomas, J.L., Law, K.S., Quennehen, B., Ancellet, G. et al. (2015) Transport of anthropogenic and biomass burning aerosols from Europe to the Arctic during spring 2008. *Atmospheric Chemistry and Physics*, 15(7), 3831–3850. Available from: https://doi.org/10.5194/acp-15-3831-2015

Masson-Delmotte, V., Zhai, P., Pirani, A., Connors, S.L., Péan, C.S., Berger, S. et al. (2021) *Climate change 2021: the physical science basis. Contribution of working group I to the sixth assessment report of the Intergovernmental Panel on Climate Change*. Geneva: IPCC.

Melfi, S.H., Spinhirne, S.-H., Chou, S.-H. & Palm, S.P. (1985) Lidar observations of vertically organized convection in the planetary boundary layer over the ocean. *Journal of Climate and Applied Meteorology*, 24, 806–821.

Münkel, C. (2007) Mixing height determination with lidar ceilometers—results from Helsinki testbed. *Meteorologische Zeitschrift*, 16(4), 451–459. Available from: https://doi.org/10.1127/0941-2948/2007/0221

Münkel, C., Schäfer, K. & Emeis, S. (2011) Adding confidence levels and error bars to mixing layer heights detected by ceilometer. *Remote Sensing of Clouds and the Atmosphere*, XVI, 817708. Available from: https://doi.org/10.1117/12.898122

Nguyen, Q.T., Glasius, M., Sørensen, L.L., Jensen, B., Skov, H., Birmili, W. et al. (2016) Seasonal variation of atmospheric particle number concentrations, new particle formation and atmospheric oxidation capacity at the high Arctic site Villum Research Station, Station Nord. *Atmospheric Chemistry and Physics*, 16(17), 11319–11336. Available from: https://doi.org/10.5194/acp-16-11319-2016

Nilsson, E.D. (1996) Planetary boundary layer structure and air mass transport during the International Arctic Ocean Expedition 1991. *Tellus, Series B: Chemical and Physical Meteorology*, 48(2), 178–196. Available from: https://doi.org/10.1034/j.1600-0889.1996.t01-1-00004.x

Overland, J.E. (1985) Atmospheric boundary layer structure and drag coefficients over sea ice. *Journal of Geophysical Research*, 90(C5), 9029–9049. Available from: https://doi.org/10.1029/JC090iC05p09029

Pauscher, L., Vasiljevic, N., Callies, D., Lea, G., Mann, J., Klaas, T. et al. (2016) An inter-comparison study of multi- and DBS lidar measurements in complex terrain. *Remote Sensing*, 8(9), 782. Available from: https://doi.org/10.3390/rs8090782

Pernov, J., Beddows, D., Jensen, D., Dall'Osto, B., Harrison, R., Skov, H. et al. (2022) Increased aerosol concentrations in the High Arctic attributable to changing atmospheric transport patterns. *npj Climate and Atmospheric Science*, 5, 62. https://doi.org/10.1038/s41612-022-00286-y

Persson, P. (2012) Onset and end of the summer melt season over sea ice: thermal structure and surface energy perspective from SHEBA. *Climate Dynamics*, 39(6), 1349–1371. Available from: https://doi.org/10.1007/s00382-011-1196-9

Persson, P., Fairall, C.W., Andreas, E.L., Guest, P.S. & Perovich, D.K. (2002) Measurements near the atmospheric surface flux group tower at SHEBA: near-surface conditions and surface energy budget. *Journal of Geophysical Research: Oceans*, 107(10), 1–35. Available from: https://doi.org/10.1029/2000jc000705

Prospero, J.M., Bullard, J.E. & Hodgkins, R. (2012) High-latitude dust over the North Atlantic: inputs from Icelandic proglacial dust storms. *Science*, 335(6072), 1078–1082. Available from: https://doi.org/10.1126/science.1217447

Prytherch, J. & Tjernström, M. (2020) *Ceilometer backscatter, cloud base height and cloud fraction data from the Arctic Ocean 2018 expedition. Dataset version 2.0*. Stockholm: Bolin Centre Database. Available from: https://doi.org/10.17043/ao2018-ceilometer-2

Raatz, W.E., Schnell, R.C. & Bodhaine, B.A. (1985) The distribution and transport of pollution aerosols over the Norwegian Arctic on 31 March and 4 April, 1983. *Atmospheric Environment*, 19(12), 2135–2142. Available from: https://doi.org/10.1016/0004-6981(85)90121-0

Sathe, A. & Mann, J. (2013) A review of turbulence measurements using ground-based wind lidars. *Atmospheric Measurement Techniques*, 6(11), 3147–3167. Available from: https://doi.org/10.5194/amt-6-3147-2013

Schmithüsen, H. (2021) *Ceilometer CL51 raw data measured during POLARSTERN cruise PS122/5 in 2020 into the Arctic Ocean. The data are deposited in the World Data Center PANGAEA hosted by the Alfred Wegener Institute (AWI) and University of Bremen (MARUM)*. Available from: https://doi.pangaea.de/10.1594/PANGAEA.929532

Seibert, P., Beyrich, F., Gryning, S.E., Joffre, S., Rasmussen, A. & Tercier, P. (2000) Review and intercomparison of operational methods for the determination the mixing height. *Atmospheric Environment*, 34, 1001–1027.

Serreze, M.C., Walsh, J.E., Chapin, F.S., III, Osterkamp, T., Dyurgerov, M., Romanosky, V. et al. (2000) Observational evidence of recent change in the northern high-latitude environment. *Climatic Change*, 46(1/2), 159–207.

Shupe, D. (2010) *Ceilometer cloud base height measurements taken at Summit Station, Greenland—Arctic Observing Network Program ARCTIC*. Available from: https://doi.org/10.18739/A2S17ST12

Stohl, A. (2006) Characteristics of atmospheric transport into the Arctic troposphere. *Journal of Geophysical Research: Atmospheres*, 111(11), 1–17. Available from: https://doi.org/10.1029/2005JD006888

Sun, J., Nappo, C.J., Mahrt, L., Belušic, D., Grisogono, B., Stauffer, D.R. et al. (2015) Review of wave-turbulence interactions in the stable atmospheric boundary layer. *Reviews of Geophysics*, 53(3), 956–993. Available from: https://doi.org/10.1002/2015RG000487

Suomi, I., Lüpkes, C., Hartmann, J., Vihma, T., Gryning, S.-E. & Fortelius, C. (2016) Gust factor based on research aircraft measurements: a new methodology applied to the Arctic marine boundary layer. *Quarterly Journal of the Royal Meteorological Society*, 142(701), 2985–3000.

Tjernström, M. (2005) The summer Arctic boundary layer during the Arctic Ocean Experiment 2001 (AOE-2001). *Boundary-Layer Meteorology*, 117(1), 5–36. Available from: https://doi.org/10.1007/s10546-004-5641-8

Tjernström, M., Shupe, M.D., Brooks, I.M., Persson, P.O.G., Prytherch, J., Salisbury, D.J. et al. (2015) Warm-air advection, air mass transformation and fog causes rapid ice melt. *Geophysical Research Letters*, 42(13), 5594–5602. Available from: https://doi.org/10.1002/2015GL064373

Tobo, Y., Adachi, K., Demott, P.J., Hill, T.C.J., Hamilton, D.S., Mahowald, N.M. et al. (2019) Glacially sourced dust as a potentiallly significant source of ice nucleating particles. *Nature Geoscience*, 12, 253–258. Available from: https://doi.org/10.1038/s41561-019-0314-x

Tomasi, C., Vitale, V., Lupi, A., Di Carmine, C., Campanelli, M., Herber, A. et al. (2007) Aerosols in polar regions: a historical overview based on optical depth and in situ observations. *Journal of Geophysical Research Atmospheres*, 112(16), D16205. Available from: https://doi.org/10.1029/2007JD008432

Uzan, L., Egert, S. & Alpert, P. (2016) Ceilometer evaluation of the eastern Mediterranean summer boundary layer height-first study of two Israeli sites. *Atmospheric Measurement Techniques*, 9(9), 4387–4398. Available from: https://doi.org/10.5194/amt-9-4387-2016

Vihma, T., Hartman, J. & Lüpkes, C. (2003) A case study of an on-ice air flow over the Arctic marginal sea-ice zone. *Boundary-Layer Meteorology*, 107(1), 189–217. Available from: https://doi.org/10.1023/A:1021599601948

Warneke, C., Froyd, K.D., Brioude, J., Bahreini, R., Brock, C.A., Cozic, J. et al. (2010) An important contribution to springtime Arctic aerosol from biomass burning in Russia. *Geophysical Research Letters*, 37(1), L01801. Available from: https://doi.org/10.1029/2009GL041816

Wiegner, M., Madonna, F., Binietoglou, I., Forkel, R., Gasteiger, J., Geiß, A. et al. (2014) What is the benefit of ceilometers for aerosol remote sensing? An answer from EARLINET. *Atmospheric Measurement Techniques*, 7(7), 1979–1997. Available from: https://doi.org/10.5194/amt-7-1979-2014

Zhu, X., Tang, G., Hu, B., Wang, L., Xin, J., Zhang, J. et al. (2016) Regional pollution and its formation mechanism over North China Plain: a case study with ceilometer observations and model simulations. *Journal of Geophysical Research*, 121(24), 14574–14588. Available from: https://doi.org/10.1002/2016JD025730

How to cite this article: Gryning, S.-E., Batchvarova, E., Floors, R., Münkel, C., Sørensen, L. L., & Skov, H. (2023). Observed aerosol-layer depth at Station Nord in the high Arctic. *International Journal of Climatology*, *43*(7), 3247–3263. https://doi.org/10.1002/joc.8027